ISSN 0915-633X

NATIONAL INSTITUTE FOR FUSION SCIENCE

Giant Charge Inversion of a Macroion Due to Multivalent Counterions and Monovalent Coions: Molecular Dynamics Study

M. Tanaka and A. Yu Grosberg

(Received - Dec. 6, 2000)

NIFS-678 Jan. 2001

RESEARCH REPORT
NIFS Series

TOKI, JAPAN

Giant Charge Inversion of a Macroion Due to Multivalent Counterions and Monovalent Coions: Molecular Dynamics Study

Motohiko Tanaka[1], and A.Yu Grosberg[2]
[1] *National Institute for Fusion Science, Toki 509-5292, Japan*
[2] *Department of Physics, University of Minnesota, Minneapolis, MN 55455*

We report molecular dynamics simulation of the (overall neutral) system consisting of an immobile macroion surrounded by the electrolyte of multivalent counterions and monovalent coions. As expected theoretically, counterions adsorb on the macroion surface in the amount much exceeding neutralization requirement, thus effectively inverting the sign of the macroion charge. We find two conditions necessary for charge inversion, namely, counterions must be multivalently charged and Coulomb interactions must be strong enough compared to thermal energy. On the other hand, coion condensation on the macroion suppresses the amount of charge inversion Depending on parameters, we observe inverted charge up to about 200% the original charge of the macroion in absolute value. The inverted charge scales as $\sim \xi^{1/2}$ when $\xi < 1$ and crosses over to $\sim \xi$ for $\xi > 1$, where $\xi = (R/r_s)^2$, R and r_s being the distance between the macroion and adsorbed counterions and the Debye screening length in the electrolyte under neutralizing conditions, respectively. These findings are highly consistent with the theory of "giant charge inversion" [*Phys.Rev Lett.,85*, 1568 (2000)].

Keywords: Nonlinear Debye screening, Coulomb coupling parameter, multivalent ions, condensation

I. INTRODUCTION

Correlation effects in the systems of charged particles, such as plasma or electrolyte solution, are well known since the works by Debye and Hückel in 1923 [1]. Classical intuition suggests that correlation can be viewed as screening in which a cloud of ions around, say, positive particle is slightly dominated by negative counterions, such that for an outside observer (who measures the electric field) the shield of predominantly negative charges effectively reduces the central positive charge. Recently, a significant attention has been attracted by the notion that much more dramatic effect is possible in the system with strongly charged ions [2]. Namely, instead of charge reduction due to the shielding it is possible to observe charge inversion due to the "over-screening". Furthermore, it was shown a year ago that the inverted charge may be quite large, even larger in absolute value than the original bare charge, giving rise to the concept of "giant" charge inversion [3].

In the present paper, we use molecular dynamics simulation technique to address the question of possible limits of charge inversion. Overall, we confirm the theoretical prediction [3] and observe "giant" charge inversion, with the ratio of inverted and bare charges reaching up to about 1.6 (in absolute value).

Although we consider here only primitive schematic model with spherical ions immersed in the medium of a constant dielectric permeability ϵ, this should be viewed as the step towards better understanding of such first magnitude scientific problems as, e.g., that of chromatin structure. Indeed, chromatin represents a complex of strongly negatively charged thread of DNA with positively charged smaller protein molecules. For instance, virtually every paper on charge inversion mentions the fact that protein core of a nucleosome particle [4] carries lesser amount of positive charge than the amount of negative charge on the wrapped around DNA. On a simpler level, complexes of polycations and polyanyons were under scrutiny for a long time [5], as well as complexes of charged polymers with charged colloids [6].

In theoretical aspect, the most advanced treatment of charge inversion is due to Shklovskii and his co-workers [3]. In their works, the universal physical mechanism behind charge inversion is recognized as correlations between shielding ions. In the first works [2], this gave rise to the idealized image of these shielding counterions forming a Wigner crystal on the surface of the shielded macroion. In most real cases, correlations are not quite as strong as to produce a crystal, but sufficient to maintain short range order, and, therefore, correlation energy is similar to that of a crystal. Obviously, this mechanism is operational when shielding ions are strongly charged. Furthermore, it was realized that the best situation for charge inversion occurs when monovalent salt is present in addition to strongly charged ions. Salt ions, as their charges are small, behave in a "traditional" way, they simply screen all interactions at the distance about Debye length r_s. However trivial itself, this leads to a dramatic increase of charge inversion, because the attraction of a counterion to its Wigner-Seitz cell on the macroion surface is over a significantly shorter range than the repulsion of a counterion from the uncompensated charge of all other counterions.

Charge inversion has been seen several times in simulations, starting from the pioneering work [7]. In recent works [8–12] computer simulations were reported along with various ways to re-derive and re-examine the concept of lateral correlations between counterions as the driving force behind charge inversion. The authors of [11,12] reported quite impressive agreement between the-

oretical conjectures and their computation data. However sophisticated, these simulations concentrated on the cases of no added salt and of abundance of counterions. In other words, they only examined the very dilute extreme with respect to macroions assuming at the same time finite concentration of counterions. Our first intent in the present work is to relax this serious restriction and to simulate a realistic model in which thermodynamic cost of adsorption of counterions on the surface of a macroion is contributed by both the events on the macroion surface and in the surrounding solution.

The other closely connected goal of our present study has to do with the following delicate aspect of the "giant" charge inversion scenario. In order to make correlations and charge inversion stronger, one is tempted to choose larger ratio of Coulomb energy to thermal energy, but when it is too large, the small salt ions start to condense on the surfaces of counterions effectively reducing their charge. Therefore, charge inversion is expected to be the strongest in the intermediate regime, when correlations between counterions are already strong, but condensation of small ions on them is still weak. Therefore, we want to check in the present work computationally how robust is this theoretical prediction.

To achieve the above stated goals, we perform in the present paper molecular dynamics study of the system consisting of a single macroion, large number of multivalent counterions, and a multitude of monovalent coions immersed in a Langevin fluid. It is worth noting that hydrodynamic effects, which may be of significant importance for interactions between colloidal particles away from thermodynamic equilibrium [13–15], are totally ignored in the present study, because we concentrate on the equilibrium aspects only.

The paper is organized as follows. The simulation method and parameters are described in Section II. In Section III, by direct measurement of the peak height of the radial charge distribution we show that giant charge inversion takes place when the following two conditions are simultaneously met: (1) Coulomb energy prevails over the thermal energy at the length scale of a single ion size, a: $\Gamma = e^2/\epsilon a k_B T > 1$, and (2) multivalent counterions with valence $Z_{ci} \geq 2$ are present. We study in details the dependence of charge inversion on the radius and charge of the macroion, the valence and density of counterions and coions, and temperature. For large density and valence of counterions, the amount of inverted charge increases linearly with density, and reaches up to 200% the original macroion charge.

Extension of the present work to the case under electrophoretic environments is discussed in a separate paper [16] in which the effect of an applied electric field on the charge inversion process is investigated with the use of molecular dynamics simulation.

II. SIMULATION METHOD AND PARAMETERS

Specifically, we consider the following model. The system includes: a single macroion with negative charge $Q_{mac} < 0$, some N^+ multivalent counterions with a positive charge $Z_{ci}e$ each, and some N^- monovalent coions with a negative charge $(-e)$ each ($e > 0$ is the elementary charge). Overall charge neutrality is strictly enforced: $Q_{mac} + N^+ Z_{ci} e - N^- e = 0$. All ions are confined within the three-dimensional simulation domain having spherical shape with radius R_{max}. The macroion is considered immobile; it is placed at the origin (center of the domain), and all other ions are mobile. All ions are supposed to be of spherical shapes, with macroion having radius R_{mac} and all mobile ions having identical radius a; a serves also as a unit of length.

The (classical) molecular dynamics simulation solves the Newton-Langevin equations of motion

$$\begin{aligned} m\frac{d\mathbf{v}_i}{dt} &= -\nabla\Phi(\mathbf{r}_i) - \nabla\phi(\mathbf{r}_i) - \nu a \mathbf{v}_i + \mathbf{F}_{th} \ , \\ \frac{d\mathbf{r}_i}{dt} &= \mathbf{v}_i \ , \end{aligned} \tag{1}$$

where the potentials Φ and ϕ, describe interactions of a given ion with other mobile ions and with the macroion, respectively:

$$\begin{aligned} \Phi(\mathbf{r}_i) &= \sum_j \left\{ \frac{Z_i Z_j e^2}{\epsilon r_{ij}} + \epsilon_{LJ} \left(\left(\frac{a}{r_{ij}}\right)^{12} - \left(\frac{a}{r_{ij}}\right)^{6} \right) \right\} \ ; \\ \phi(\mathbf{r}_i) &= Z_i e \, \frac{Q_{mac}}{\epsilon r_i} \ . \end{aligned} \tag{2}$$

Here, $\mathbf{r}_i$ and $\mathbf{v}_i$ are the position and velocity vectors of the i-th particle, $r_{ij} = |\mathbf{r}_i - \mathbf{r}_j|$, ϵ the dielectric constant, ϵ_{LJ} the Lennard-Jones energy. As regards boundaries, we assume elastic reflection every time when a mobile ion hits either the domain boundary at $r = R_{max}$ or the macroion surface at $r = R_{mac}$. The last two terms of Eq.(1) represent the Langevin thermostat due to surrounding neutral medium. The Stokes formula for a sphere is adopted for the friction term with ν being the friction constant, and $\mathbf{F}_{th}$ is the random δ-correlated thermal agitation.

The inertia term is retained in the momentum equation for numerical stability of the electrostatic forces, masses of all mobile ions are assumed identical, equal to m. This leads to the choice of ω_p^{-1} as the natural time unit, where $\omega_p = (4\pi n_0 e^2/\epsilon m)^{1/2}$ is plasma frequency and n_0 the average ion number density.

It must be born in mind that phenomena resembling charge inversion may occur when other forces, apart from Coulomb electrostatic ones, operate in the system (including complicated helical shape of the molecules involved; see, for instance, [17]). In this study we are interested in the situation when pure electrostatic forces dominate. Accordingly, we choose $\epsilon_{LJ} = (1/12)e^2/\epsilon a$;

this corresponds to the depth of Lennard-Jones potential well equal to $-\epsilon_{LJ}/4 = -(1/48)e^2/\epsilon a$, which means that Lennard-Jones attraction force is very small compared to Coulomb force. The latter is characterized by the Coulomb coupling parameter $\Gamma = e^2/\epsilon a T$, where T is temperature in the energy unit (the Boltzmann constant k_B is omitted). Another way to view Γ is to note that Bjerrum length (the length at which Coulomb energy is equal to T) is equal to $\ell_B = \Gamma a$. In the present study, we typically look at the Γ values in the range $\Gamma = 3 \sim 11$ The particular values,

$$m \approx 50 m_H \ , \quad a \approx 2\mathring{A} \ , \quad n_0 \approx 1/(10\mathring{A})^3, \quad \epsilon \approx 80 \quad (3)$$

give rise to $\Gamma \approx 3.5$ for $T \approx 300K$, and $\omega_p \approx 7.4 \times 10^{11} s^{-1}$ or $\omega_p^{-1} \approx 1.4ps$, where m_H is proton mass, and n_0 the average density of counterions.

The initial positions of co- and counterions are distributed randomly between the two spheres $R_{mac} < r < R_{max}$, each ions having the velocity that satisfies the Maxwell distribution. The integration of the equations of motion is done with the use of the leapfrog method which is equivalent to Verlet algorithm [18]. The time step of integration is $\Delta t = 0.01\omega_p^{-1}$, and simulation runs are executed up to $5000\omega_p^{-1}$ at which time the peak height of the inverted charge Eq.(7) has become stationary.

Below, in Section III, we report the results of simulations concentrating on the general properties of the charge inversion: its dependence on the radius and charge of a macroion, the valence and density of counterions, and temperature. While changing the parameters, the electrostatic binding energy of counterions to the macroion is kept constant by fixing $\Gamma_Q = |Q_{mac}|e/\epsilon R_{mac} T$.

In the present study, the following values of parameters are considered "standard" and used unless otherwise specified: radius of the macroion $R_{mac} = 3a$, its charge $Q_{mac} = -28e$ (assumed negative), valence of the counterions $Z_{ci} = 7$, and the number of the counterions and coions $N^+ = 52$ and $N^- = 336$, respectively. The radius of the outer boundary sphere is $R_{max} = 20a$. The temperature is chosen such that Coulomb coupling parameter is $\Gamma = 4.2$.

To support physical intuition, it is useful to note that under the "standard" conditions the Debye screening length,

$$r_s = \left[4\pi e^2 \frac{{Z_{ci}}^2 N^+ + N^-}{\frac{4}{3}\pi(R_{max}^3 - R_{mac}^3)\epsilon T} \right]^{-1/2} = a \left[\frac{(R_{max}/a)^3 - (R_{mac}/a)^3}{3\Gamma\left({Z_{ci}}^2 N^+ + N^-\right)} \right]^{1/2}, \quad (4)$$

is about $0.5a$. At the same time, Gouy-Chapman length associated with the surface of a macroion,

$$\lambda = \frac{\epsilon T}{2\pi e \sigma} = a \frac{2(R_{mac}/a)^2}{\Gamma |Q_{mac}/e|} \quad (5)$$

(where $\sigma = |Q_{mac}| / 4\pi R_{mac}^2$) turns out to be about $0.15a$. (Strictly speaking, λ is defined for the plane, not spherical, surface; however, since $\lambda/R_{mac} \approx 0.05 \ll 1$, defining λ based on plane geometry is reasonable.) It may also be noted that Bjerrum length is equal to Γa, which is $4.2a$ in our standard case. These values of parameters, particularly $r_s < a$, are chosen because they correspond to the regime in which theory [3] predicts the most significant charge inversion effect.

It should be also noted that volume fraction of particles in the simulation domain, $\phi = a^3(N^+ + N^-)/(R_{max}^3 - R_{mac}^3)$, is small: for the standard case parameters, it is $\phi \approx 0.05$; it is also small in other cases considered in this paper. Thus, non-Coulomb interactions between ions are not so significant. On the other hand, Coulomb interactions are strong. For instance, the parameters controlling validity of the linearized Debye-Hückel theory for the plasma away from macroion are $Z_{ci}^2 \phi_+^{1/3} \Gamma$ and $Z_{co} \phi_-^{1/3} \Gamma$, and they are both large compared to unity, about 10–200 (Z_{ci}=3–7) and 1–4, respectively. (These parameters mean ratio of Coulomb and thermal energies at typical distances - controlled by densities - between particles of respective signs.) Thus, we consider the conditions under which plasma outside the macroion is very nonlinear.

For the standard run, it takes about $2.5 \times 10^3 \omega_p^{-1}$ before a state is reached which can be assumed equilibrated, at least in terms of the inverted charge being stationary.

III. SIMULATION RESULTS

A. Observing charge inversion

1. Standard regime

The results of our simulations are presented in the Figures 1–8. Figure 1 gives a typical results of a run performed under what we call "standard" conditions. Specifically, we show a snapshot of the spatial distribution of counterions and coions around the macroion after charge distribution has become stationary. Since our simulation includes hundreds of particles, it is impossible to "see" them in any meaningful way; what we can see, however, is the configuration of ions in the immediate vicinity of the macroion surface. This is shown in Fig.1(a) in which only the ions residing in the thin layer $R_{mac} \le r \le R_{mac} + 3a$ are depicted.

As seen in Fig.1(a), counterions (light grey) attach right on the surface of the macroion with a lateral spacing, while coions (dark grey) stay some distance away from the macroion surface. It is clear that lateral correlations are present between counterions, particularly because there are no pairs in which counterions are closely approaching each other. Not surprisingly, however, this correlations are much weaker than in the case without

coions examined in [12]: although counterions are correlated in the Fig.1(a), their spacings are not regular and cannot be identified as Wigner crystal. As regards coions, they are seen to condense on the top side of the counterions, presumably because of strong repulsion of the coions from macroion surface. We note here that this condensation of coions on the counterions is the process of limiting the amount of charge inversion. In the configuration shown in the Fig.1(a), the numbers of counterions and coions within the distance a from the macroion surface are $N^+ = 11$ and $N^- = 5$, respectively. This means that the net charge of the entire complex, i.e. "macroion + attached counterion + attached coions", is $+44e$. This is to be compared with the bare macroion charge of $-28e$, which amounts to charge inversion of about 160% the original macroion charge.

Figure 1(b) shows the radial distributions of co- and counter-ions charges

$$q_s(r) = eZ_s \int \sum_{i \in s} \frac{\delta(\mathbf{r} - \mathbf{r}_{si})}{4\pi r_{si}^2} d\Omega_{\mathbf{r}} \ , \qquad (6)$$

where s means either co- or counter-ions, Z_s is, accordingly, either -1 or Z_{ci}; summation runs over all ions of the given sort s, $\mathbf{r}_{si}$ is the position vector of ion i of the sort s, and $\Omega_{\mathbf{r}}$ is the solid angle of directions of vector $\mathbf{r}$. These results are consistent with the conclusion of 160 % charge inversion. Indeed, the distribution of the counterions, denoted by open bars, is sharply peaked at $r \cong R_{mac}$, while that of the coions (shaded bars) is broad and detached from the macroion surface. Although at this stage we do not formulate any rigorous algorithmic definition as to which counterions are close enough to the macroion to be called "bound," we note that the peak in the radial density distribution of counterions is sharp enough to provide for quite clear distinction between bound and unbound ions. We therefore rely on this sharp peak, and in what follows we describe as bound those counterions which belong to this peak.

Figure 1(c) depicts the integrated charge of the movable ion species (counterions and coions) of Fig.1(b), starting at the surface of the macroion,

$$Q(r) = \sum_s \int_{R_{mac}}^{r} q_s(r') \ 4\pi \ r'^2 \ dr' \ . \qquad (7)$$

The portion above the baseline $Q/|Q_{mac}| = 1$ corresponds to the charge inversion (this applies to all the following figures). The net amount of inverted charge reaches 160% for this run, as stated above, and the $Q(r)$ profile relaxes to neutrality in a distance of approximately few a, thus suggesting once again that a significant population of coions reside on the outer sides of condensed counterions. Fluctuations of $Q(r)$ for $r \gg R_{mac}$ reflect density fluctuations, which are much amplified because of the volume factor $4\pi r^2$. On the other hand, we observe a nearly neutral region $Q/|Q_{mac}| \approx 1$ extending for the distance comparable to the Bjerrum length ℓ_B outside the charge inversion layer. Few ions exist in this region. This shows establishment of enhanced order due to strong Coulomb interactions.

The electrostatic potential drop across the charge distribution peak corresponds to energy change $e\Delta\varphi \approx 1.2e^2/\epsilon a$, which is five times the thermal energy $k_BT = e^2/\epsilon a\Gamma$. This implies strong binding of counterions to the macroion and coions to the counterions, or, in other words, this manifests very strongly non-linear screening compared with Debye-Hückel screening of weakly coupled cases. Of course, this is by no means surprising given the small value of λ, as mentioned above, Eq. (5).

Speaking about the dynamics of equilibration, it is interesting to note that the buildup of counterions on the macroion occurs fairly quickly, in about $100\omega_p^{-1}$, which is of the order of 100 picosec for the typical numerical values of parameters, as suggested in Eq. (3). This time is much shorter than overall relaxation time of the system, suggesting that equilibration of plasma further away from macroion occurs fairly slowly. It is appealing to guess that this fast buildup of screening (and even over-charging) layer is connected with the fact of strongly non-linear correlated screening.

2. Other regimes

The charge inversion for the macroion with a large radius $R_{mac} = 8a$ is depicted in Fig.2. Other parameters are the same as those of Fig.1, except for the lower temperature ($\Gamma = 11.2$) to keep the Coulomb coupling parameter $\Gamma_Q = const$. We again observe sparsely distributed counterions on the macroion surface. In this case, however, binding of the counterions to the macroion is loose, and their radial distribution in Fig.2(b) is almost as broad as that of the coions. The counterion charge is better canceled on each site by the condensed coions than in Fig.1. We note that the number of condensed ions to the macroion surface in Fig.2 is $N^+ \sim 13$ and $N^- \sim 66$, where the number of N^+ is comparable to that in Fig.1. This is consistent with the fact that each counterion occupies, roughly, a neutralizing region on the macroion surface, similar to the Wigner-Seitz cell of Wigner crystal. With charge density of the macroion surface $\sigma = Q_{mac}/4\pi R_{mac}^2$, the size of such neutralizing region, or cell, is proportional to the size of the macroion: $eZ_{ci} = \pi\sigma R_{ws}^2$, or $R_{ws} = 2R_{mac}(Z_{ci}e/|Q_{mac}|)^{1/2}$. In other words, the neutralizing number of counterions $(R_{mac}/R_{ws})^2$ stays unchanged as long as the macroion charge Q_{mac} is fixed. The inverted charge in Fig.2(c) is about 40% the original charge of the macroion, which is less than that in Fig.1. The electrostatic potential drop across the macroion surface is consistently less than the thermal energy, $e\Delta\varphi \sim 0.05e^2/\epsilon a < k_BT \sim 0.09e^2/\epsilon a$.

The linear Debye-Hückel theory nearly applies in this case.

We found similar features, based on identification of bound ions in the peak of their radial distribution, also for the parameters further away from our standard conditions. For instance, we mention here in passing the case of the counterions with smaller valence $Z_{ci} = 3$. For them, it takes somewhat less than $1 \times 10^3 \omega_p^{-1}$ to reach the stationary state, and the attained peak height is lower, about 70% the macroion charge, as shown in Fig.6 This will be discussed in greater details in one of the sections below.

B. Changing macroion properties and temperature

In the following figures, Figs.3–7, the ordinate Q_{peak} is the maximum of the integrated charge of the counterions plus coions, Eq.(7). Each data point is an average of three runs, and a vertical bar shows the range of time variations and deviations among the runs.

The dependence of charge inversion on the radius of the macroion is depicted in Fig.3. For different values of the radius, temperature is adjusted accordingly to keep unchanged the Coulomb coupling parameter, $\Gamma_Q \propto 1/(R_{mac}T)$. The valence of the counterions is chosen either $Z_{ci} = 3$ or 7. The number of counterions is $N^+ = 121$ and $N^+ = 52$ for $Z_{ci} = 3$ and 7, respectively, which is large compared to $|Q_{mac}|/Z_{ci}e$ required for charge neutralization of the macroion. These parameters are chosen in such a way that the number of coions, which is determined by neutrality condition, is virtually fixed, being $N^- = 335$ for the $Z_{ci} = 3$ case and $N^- = 336$ for the $Z_{ci} = 7$ case. This corresponds to r_s (4) moderately changing between $0.3a \sim 0.8a$, and λ (5) changing between $0.02a \sim 2.8a$.

In Fig.3, the inverted charge reaches its maximum for the radius $R_{mac} \approx 3a$ irrespectively of the valence Z_{ci}. It falls off rapidly both for smaller and larger radii, and becomes insensitive to the radius of the macroion for $R_{mac}/a \gg 1$. The net amount of the inverted charge is about 70% of the bare macroion charge Q_{mac} for $Z_{ci} = 3$; it increases up to 150% of Q_{mac} for $Z_{ci} = 7$. The charge inversion reaches maximum also at virtually the same radius $R_{mac} \approx 3a$ even for the smaller number of counterions $N^+ = 15$ ($Z_{ci} = 7$), or for larger macroion charge $Q_{mac} = -42e$.

It is not difficult to understand qualitatively why the charge inversion decreases at both small and large values of macroion radius R_{mac}, reaching a maximum in between. When R_{mac} gets very large, the lateral spacings between bound counterions become too long to maintain correlations between them; on the other hand, when R_{mac} gets too small, the increased repulsion of the inverted charge from the macroion becomes dominant.

The effect of temperature on charge inversion is shown in Fig.4. In this figure, the abscissa is defined as $\Gamma_z = Z_{ci}e^2/\epsilon aT$. As the figure indicates, the inverted charge data for different values of valence form a master curve when plotted against Γ_z. The charge inversion is maximized at the intermediate temperature corresponding to $\Gamma_z \sim 45$, or $Z_{ci}e^2/\epsilon R_{mac}T \sim 15$ ($R_{mac} = 3a$). The value of the Debye length is $r_s \approx 0.6a$ for $Z_{ci} = 3$ and $r_s \approx a$ for $Z_{ci} = 7$. For the low temperature side, $\Gamma_z \sim 100$, the integrated charge distribution $Q(r)$ is sharply peaked as that of Fig.1(c), while at the high temperature side, $\Gamma_z \sim 10$, this distribution $Q(r)$ is rugged and fluctuates considerably with time. The maximal charge inversion is achieved through competition of counterion attachment to the macroion and coion condensation on the counterions. Lower temperatures are favored for the former due to larger Coulomb binding energy, and higher temperatures are better to suppress the latter due to enhanced thermal motion.

Figure 5 shows that charge inversion $Q_{peak}/|Q_{mac}|$ is insensitive to the charge content of the macroion Q_{mac} for fixed value of $\Gamma_Q = Q_{mac}e/\epsilon R_{mac}T$ ($\Gamma = 4.2$ or 6). The number of counterions attached to the macroion surface is in the range $8 \sim 15$ for $|Q_{mac}| = (14 \sim 42)e$ and $Z_{ci} = 7$, which is a few times that of the neutralizing number of counterions, $|Q_{mac}|/Z_{ci}e$.

We note in passing that the geometrical capacity of the surface, controlled by non-Coulomb short range forces is still very far from exhausted, $4\pi R_{mac}^2/\pi a^2 \sim 36$. The regime of closed and almost closed packing of the bound spheres on the macroion is examined in the recent work [19]. Interestingly, the *effective* valence of the counterions Z_{eff}, which is the charge of the counterion minus that of the condensed ions, increases with the charge of the macroion; it is $Z_{eff} \sim 0.25Z_{ci}$ for $Q_{mac} = -14e$ and is $Z_{eff} \sim 0.4Z_{ci}$ for $Q_{mac} = -42e$.

C. Changing counterion properties

The dependence of inverted charge on the valence of the counterions is depicted in Fig.6. Here, the macroion charge and radius are $Q_{mac} = -28e$ and $R_{mac} = 3a$, respectively, and temperature is fixed at $\Gamma = e^2/\epsilon aT = 4.2$. It is emphasized that no charge inversion is observed for monovalent counterions. The amount of the inverted charge Q_{peak} increases with the valence, which is well scaled by $Q_{peak} \sim (Z_{ci})^{1/2}$ for $Z_{ci} \leq 5$. The $Z_{ci} \geq 5$ part can be fit by $Q_{peak} \sim Z_{ci}$. The inverted charge is also an increasing function of the number of counterions and coions, as seen by the difference of the two curves for two densities in the figure.

The dependence of inverted charge on the ionic strength density of the counterions and coions, $n_I = (N^+Z_{ci}^2 + N^-)/V$ is shown in Fig.7, where $V = 4\pi R_{max}^3/3$. The amount of inverted charge $Q_{peak}/|Q_{mac}|$

increases monotonically with the ionic strength. The functional form of the scaling changes at $n_I \sim 0.05/a^3$, as shown by fitting curves. The ionic strength density of a Ca^{2+} ion and neutralizing coions in every $10\mathring{A}$ cube yields $0.048/a^3$ for $a = 2\mathring{A}$. The scaling $Q_{peak} \sim n_I^{1/2}$ for the low ionic strength densities $n_I < 0.02/a^3$ smoothly joins a linear scaling $Q_{peak} \sim n_I$ for high ionic strength densities $n_I > 0.05/a^3$. The non-dimensional parameter of the theory [3], $\zeta = (R_{ws}/r_s)^2 = 12a\Gamma N_{ci}(Z_{ci}e/|Q_{mac}|)(R_{mac}^2/R_{max}^3)$, is calculated to be 0.7 for $n_I \sim 0.01/a^3$ and $Z_{ci} = 7$. The theory expects $Q^{(th)} \sim (N_{ci}Z_{ci})^{1/2}$ for $\zeta \ll 1$, and $Q^{(th)} \sim N_{ci}Z_{ci}$ for $\zeta \gg 1$. The present simulation results agree with this theoretical prediction.

D. Measuring potential energy

The potential energy presented in Fig.8 is in line with the tendency of charge inversion dependence on variations of the Coulomb coupling parameter (cf. Fig.4). The potential energy for the interactions between counterions and the macroion (solid circles) is negative (attractive) and is minimized at the intermediate value of $Z_{ci}e^2/\epsilon aT \sim 50$ where largest charge inversion is obtained. The potential energy of interactions between the counterions and coions, depicted by triangles, decreases remarkably with the increase in $Z_{ci}e^2/\epsilon aT$. This corresponds to massive condensation of coions onto the counterions (similar to Manning-Onsager condensation) at low temperatures. This reduces the effective valence of the counterions, and the binding of counterions on the macroion surface is weakened, which tends to suppress the charge inversion. Thus, charge inversion becomes largest at the intermediate value of $Z_{ci}e^2/\epsilon aT$, as stated above. The potential energy of interaction between coions and the macroion (open circles) is positive (repulsive), and is maximized where the coions are closely located with the macroion by condensation to the counterions, namely at $Z_{ci}e^2/\epsilon aT \sim 50$. On the other hand, the total potential energy (squares) decreases with the increase in the coupling parameter $Z_{ci}e^2/\epsilon aT$.

IV. CONCLUSION

In this paper, we showed the occurrence of giant charge inversion and examined its parameter dependencies with the use of molecular dynamics simulations. The charge inversion was found to be based on the strong correlations of the multivalent counterions and coions, particularly on the surface of the macroion. Specifically, charge inversion was observed under the conditions for which the Coulomb coupling parameter was significantly larger than unity, $\Gamma = e^2/\epsilon ak_BT \gg 1$. At the same time, charge inversion occurred only in the presence of multivalent counterions with $Z_{ci} \geq 2$. The counterions were attached to the surface of the macroion, while monovalent coions tended to condense on the counterions which was the process of suppressing the amount of charge inversion. The amount of the inverted charge Q_{peak} was maximal at rather small radius of the macroion, and leveled off when radius becomes larger. It scaled linearly with the charge of the macroion Q_{mac}, and the ratio $Q_{peak}/|Q_{mac}|$ was independent of the macroion charge.

With respect to the valence Z_{ci} and the ionic strength density $n_I = (N^+Z_{ci}^2 + N^-)/V$, the amount of inverted charge scaled as $Q \sim (Z_{ci}n_I)^{1/2}$ for the valence $Z_{ci} \leq 5$ or $n_I \leq 0.02/a^3$. As noted in Sec.III C, this ionic strength density corresponds to a Ca^{2+} ion in every $10\mathring{A}$ cube. The inverted charge scaled as $Q \sim Z_{ci}n_I$ for $Z_{ci} > 5$ or $n_I > 0.05/a^3$. This agreed with the theory of giant charge inversion [3]. The net inverted charge of nearly up to 160% the bare charge of the macroion was achieved at the medium temperature $Z_{ci}e^2/\epsilon R_{mac}T \sim 15$, due to the competition of multivalent counterion attachment to the macroion and monovalent coion condensation on the counterions; the former was stronger at lower temperatures, and the latter was suppressed at higher temperatures.

In the present study, the macroion was assumed to be immobile. From the application points of view, it might be informative to study the distribution of counterions and coions around moving macroions and also the effect of an applied electric field. The study of such cases is reported in a separate paper. The results indicate that a formed complex of a macroion and counterions drifts along the electric field in the direction implied by the inverted charge, and that charge inversion is not altered until the electric field exceeds a critical value [16].

ACKNOWLEDGMENTS

The authors are highly grateful to Professor Boris I. Shklovskii whose suggestions helped them to perform the current study. We also thank him for reading the paper and giving them valuable comments.

[1] P.Debye, and E.Hückel,"On the theory of electrolytes", *Phys.Zeitsch., 24*, 185 (1923).

[2] B.I.Shklovskii, *Phys.Rev.E, 60*, 5802 (1999).

[3] T.T.Nguyen, A.Yu.Grosberg, B.I.Shklovskii, *Phys.Rev.Lett., 85*, 1568 (2000).

[4] K.Luger, A.Mader, R.Richmond, D.Sargent, T.Richmond, *Nature, 389*, 251 (1997).

[5] E.Bakeev, Yang, I.Shu, A.Zezin, V.Kabanov, A.Lezov, A.Mel'nikov, I.Kolomiets, E.Rjumtsev, W.MacKnight *Macromolec., 29*, 1320 (1996).
[6] Y. Wang, K. Kimura, Q. Huang, P. L. Dubin, W Jaeger, *Macromolec., 32*, 7128 (1999).
[7] L.Gulbrand, B.Jonsson, H.Innerstrom, and P.Linse, *J.Chem.Phys., 80*, 2221 (1984); R.Kjellander, and S. Marcelja, *Chem.Phys.Lett., 114*, 124(E) (1985)
[8] E.Allahyarov, I.D'Amico, and H.Löwen, *Phys.Rev Lett., 81*, 1334 (1998).
[9] E.M.Mateescu, C.Jeppersen, and P.Pincus, *Europhys. Lett., 46*, 454 (1999).
[10] P.Linse and V.Lobaskin, *Phys.Rev.Lett., 83*, 4208 (1999)
[11] A. G. Moreira, R. R. Netz *Europhys. Lett*, to be published; cond-mat/0009376.
[12] R.Messina, C.Holm, and K.Kremer, *Phys Rev.Lett , 85*, 872 (2000).
[13] J.C.Crocker, and D.G.Grier, *Phys.Rev.Lett., 73*, 352 (1994)
[14] G.M.Kepler, and S.Fraden, *Phys.Rev.Lett., 73*, 356 (1994).
[15] T.Squires, M.Brenner *Phys Rev.Lett., 85*, 4976 (2000).
[16] M Tanaka and A.Yu Grosberg, manuscript in preparation.
[17] A.Kornyshev, S.Leikin *Phys.Rev.Lett , 84*, 2537 (2000)
[18] For example, Understanding Molecular Simulation, D.Frenkel, and B.Smit (Academic Press, 1996)
[19] T.Nguyen, and B.Shklovskii (private communication).

FIGURE CAPTIONS

Figure 1. Charge inversion under "standard conditions": macroion radius $R_{mac} = 3a$, charge $Q_{mac} = -28e$, Coulomb coupling parameter $\Gamma = e^2/\epsilon aT = 4.2$. (a) The bird's-eye view of multivalent counterions of valence $Z_{ci} = 7$ and monovalent coions that reside within $3a$ from the macroion surface are depicted by small spheres in light and dark grey, respectively. The central large sphere represents the macroion. (b) The radial distribution function of the charge $q_s(r)$ Eq.(6) of counterions (open bars) and that of coions (shaded bars) as a function of the distance r from the macroion center. (c) The integrated charge distribution $Q(r)$ of counterions plus coions Eq.(7). The portion $Q(r)/|Q_{mac}| > 1$ corresponds to charge inversion.

Figure 2. Charge inversion for the macroion with a large radius $R_{mac} = 8a$. The plot format and other simulation parameters are the same as those of Fig.1, except that the temperature is adjusted to keep constant the electrostatic binding energy of counterions, i.e. $\Gamma = e^2/\epsilon R_{mac}T = const.$ Counterions are loosely bound to the macroion as Q_{mac} is fixed, and although the amount of inverted charge is smaller compared to that in Fig.1, it is still significant.

Figure 3. Dependence of inverted charge on the radius of macroion R_{mac} shown for the counterions with the valence $Z_{ci} = 3$ and 7. The charge of the macroion is $Q_{mac} = -28e$, and the number of coions $N_{ci}^- = 335$ (or 336) corresponds to the density $n^- \sim 1 \times 10^{-2}a^{-3}$. The ordinate is the maximum of the integrated charge $Q(r)$ (Eq.(7)), i.e. $Q_{peak} = \max(Q(r))$, normalized by the macroion charge $|Q_{mac}|$. Each data point is an average of three runs, and a vertical bar shows the range of time variations.

Figure 4. Dependence of inverted charge on temperature shown for counterions with different valence Z_{ci}, which is given by a master curve. The abscissa is the ratio of the Coulomb energy of the counterions to thermal energy, $Z_{ci}e^2/\epsilon aT$. The radius of macroion is $R_{mac} = 3a$, and the number of coions is kept nearly the same, $N_{ci}^- \sim 335$ or 336 for $Z_{ci} = 5$ and 7.

Figure 5. Dependence of inverted charge on the macroion charge Q_{mac}. The radius of macroion is $R_{mac} = 3a$, the valence of counterions is $Z_{ci} = 7$. Temperature is adjusted to keep the binding energy $\Gamma_Q = |Q_{mac}|e/\epsilon R_{mac}T$ constant as Q_{mac} varies.

Figure 6. Amount of inverted charge Q_{peak} increasing monotonically with the valence of counterions Z_{ci}. The inverted charge is well fit by $Q_{peak} \sim (Z_{ci})^{1/2}$ for $Z_{ci} \leq 5$, and $Q_{peak} \sim Z_{ci}$ for $Z_{ci} \geq 5$. Note that charge inversion occurs only for multivalent counterions, i.e. $Z_{ci} \geq 2$.

Figure 7. Dependence of inverted charge on the ionic strength density of the counterions and coions $n_I = (Z_{ci}^2 N^+ + N^-)/V$ with $V = 4\pi R_{max}^3/3$. Charge neutrality of the system is maintained. The guide curve is $n_I^{1/2}$ for $n_I < 0.02/a^3$, and n_I for $n_I > 0.05/a^3$. The macroion radius is $R_{mac} = 3a$, charge $Q_{mac} = -28e$, the valence of counterions $Z_{ci} = 7$, and the Coulomb coupling parameter $\Gamma = e^2/\epsilon aT = 4.2$.

Figure 8. Potential energy shown as a function of $Z_{ci}e^2/\epsilon aT$ for the runs with $Z_{ci} = 7$ (cf. Fig.4). The filled and open circles correspond to the potential energy of interaction of a macroion with counterions and coions, respectively, the triangles those between counterions and coions, and the squares the total potential energy.

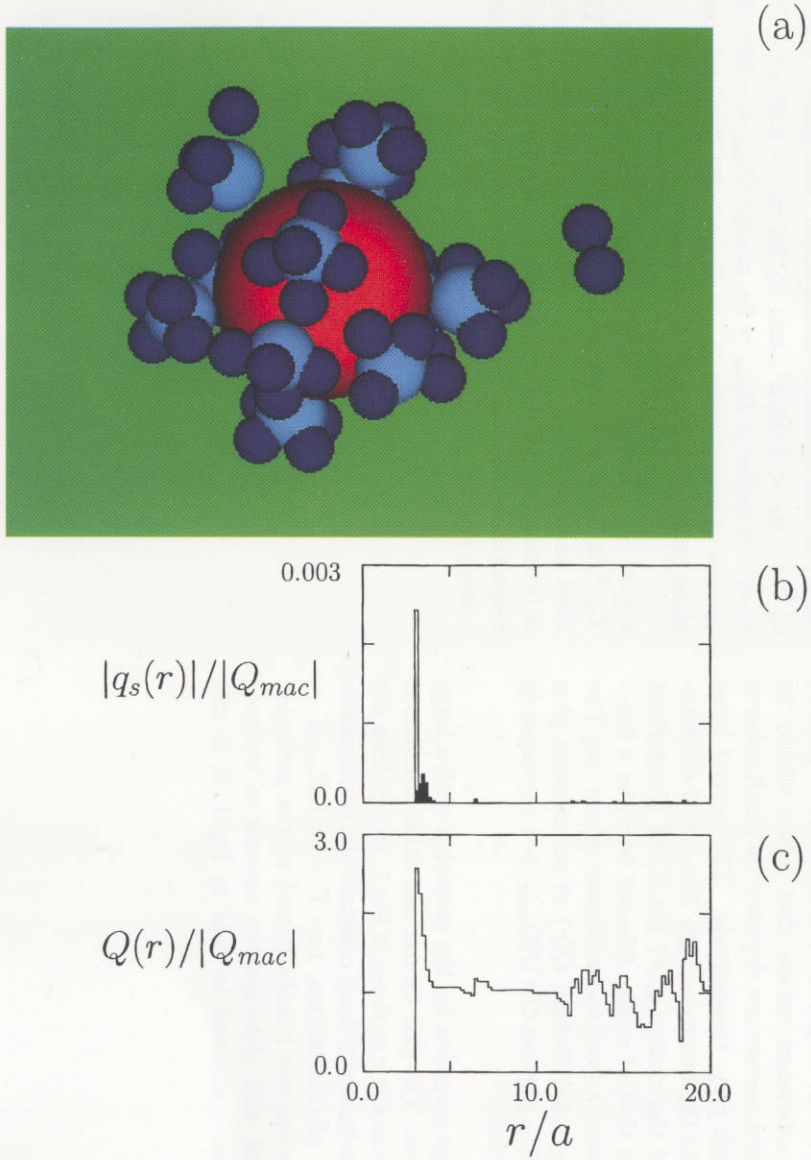

Figure 1.

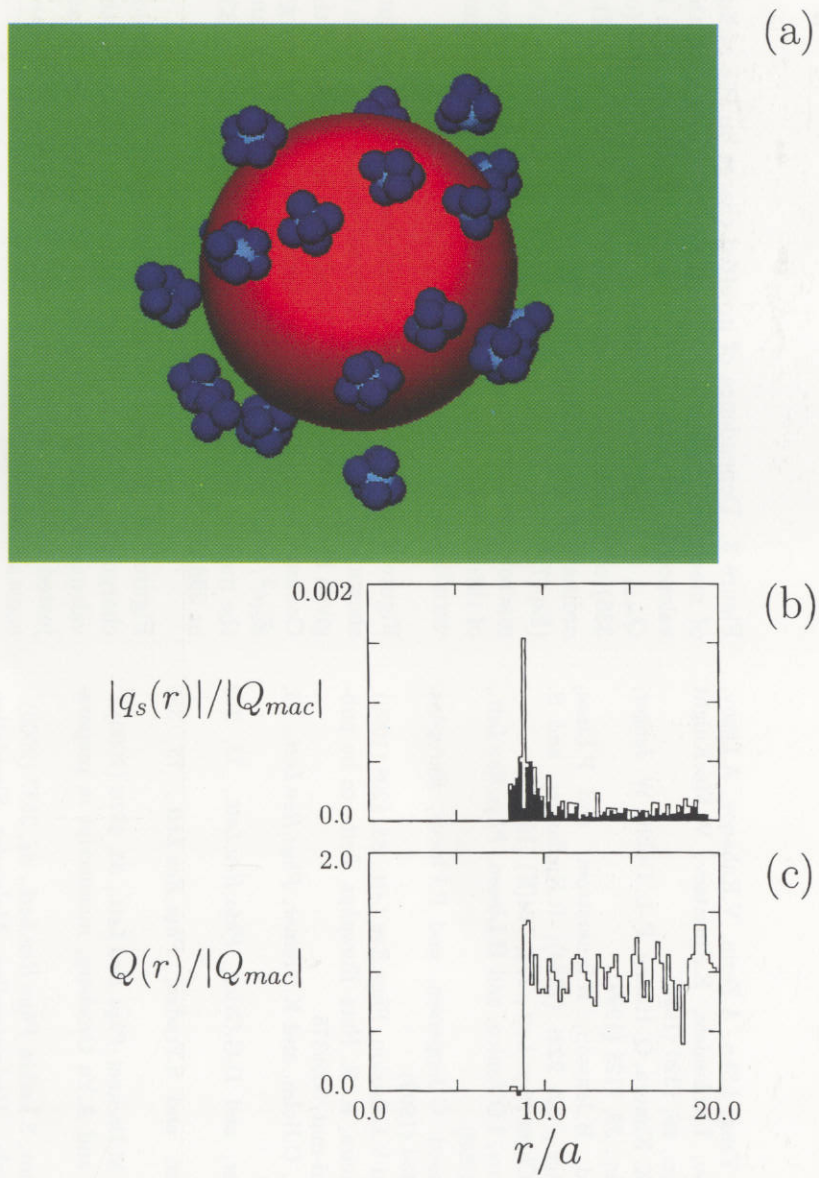

Figure 2.

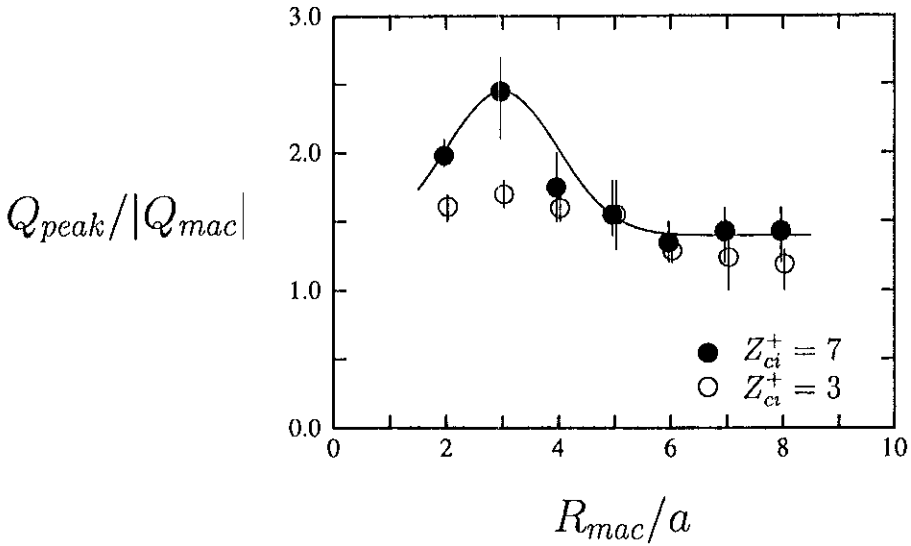

Figure 3.

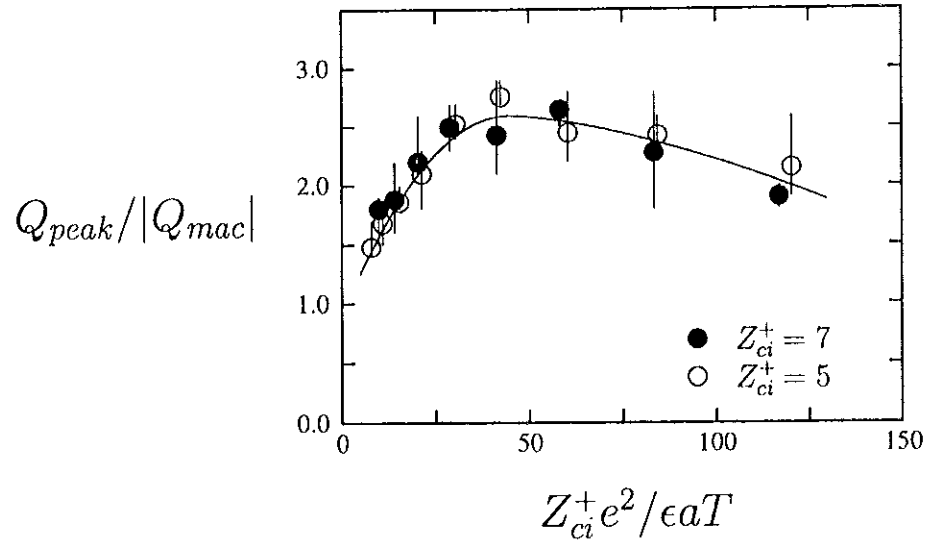

Figure 4.

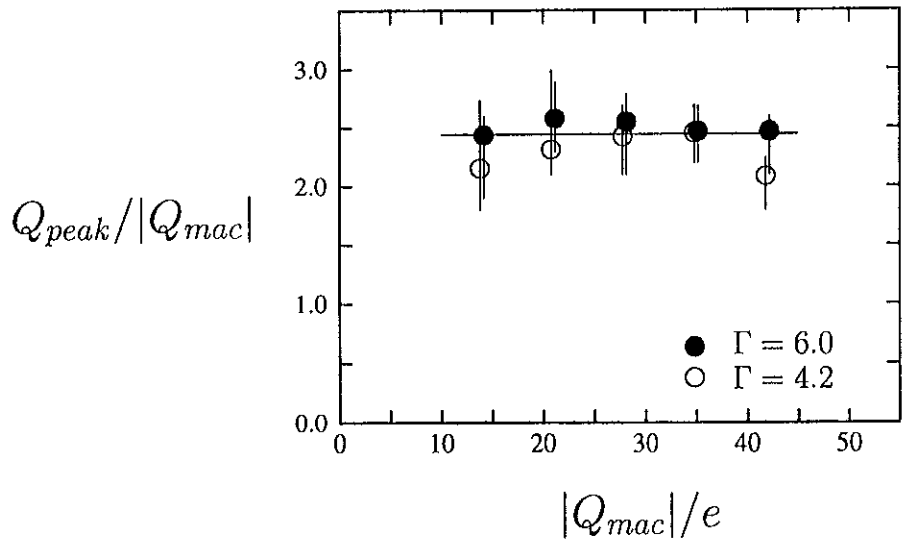

Figure 5.

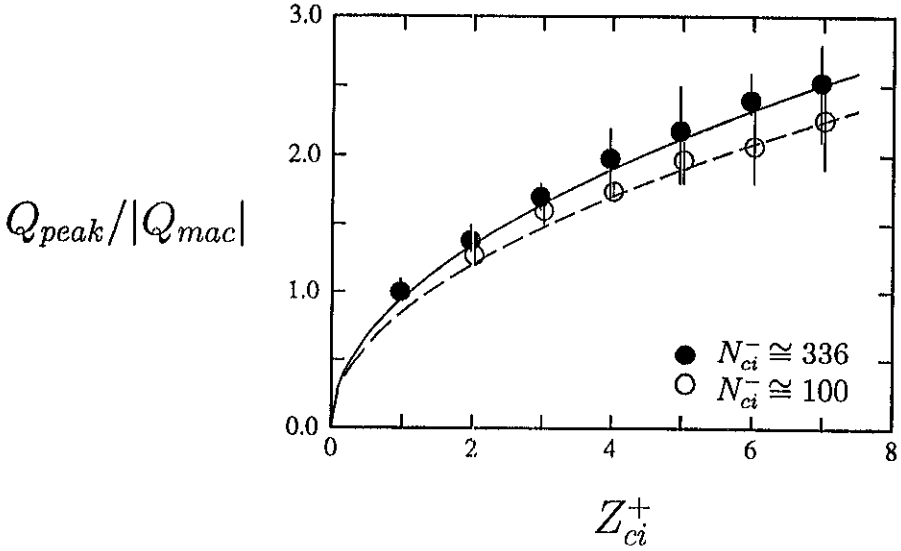

Figure 6.

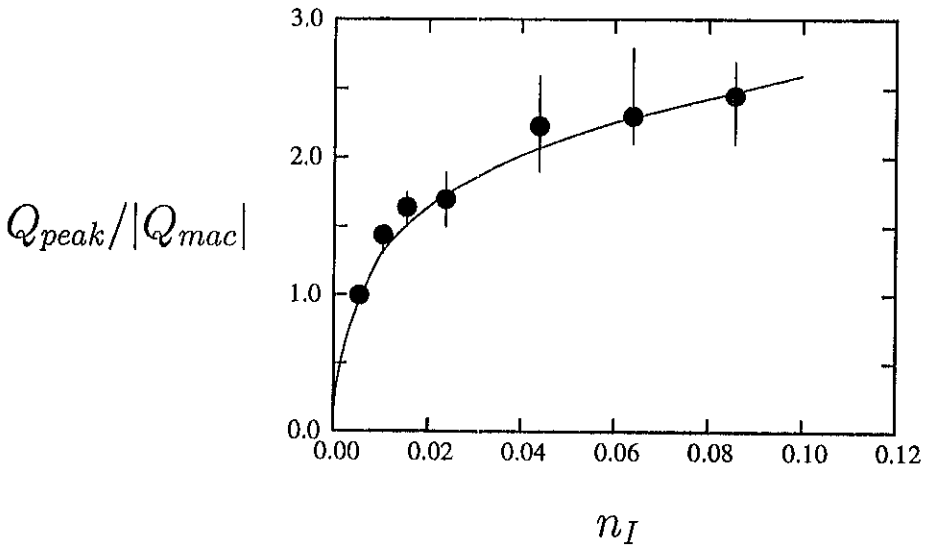

Figure 7.

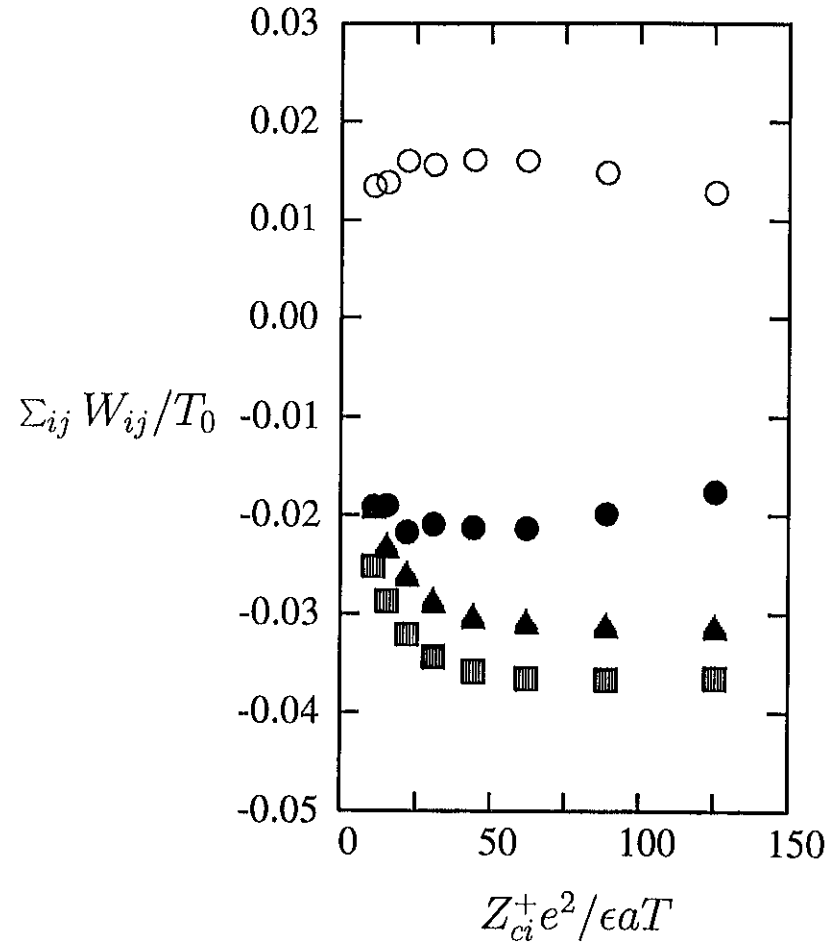

Figure 8.

Recent Issues of NIFS Series

NIFS-659 T Satow, S Imagawa, N Yanagi, K Takahata, T Mito, S Yamada, H Chikaraishi, A Nishimura, J Ohtake, Y Nakamura, S Satoh, O Motojima
Achieved Capability of the Superconducting Magnet system for the Large Helical Device Sep 2000
(IAEA-CN-77/FTP1/15)

NIFS-660 T Watari, T Mutoh, R Kumazawa, T Seki, K Saito, Y Torii, Y P Zhao, D Hartmann, H Idei, S Kubo, K Ohkubo, M Sato, T Shimozuma, Y Yoshimura, K Ikeda, O Kaneko, Y Oka, M Osakabe, Y Takeiri, K Tsumori, N Ashikawa, P C deVries, M Emoto, A Fukuyama, H Funaba, M Goto, K Ida, S Inagaki, N Inoue, M Isobe, K Itoh, S Kado, K Kawahata, T Kobuchi, K Khlopenkov, A Komori, A Krasilnikov, Y Liang, S Masuzaki, K Matsuoka, T Minami, J Miyazawa, T Morisaki, S Morita, S Murakami, S Muto, Y Nagayama, Y Nakamura, H Nakanishi, K Narihara, K Nishimura, N Noda, A TNotake, S Ohdachi, N Ohyabu, H Okada, M Okamoto, T Ozaki, R O Pavlichenko, B J Peterson, A Sagara, S Sakakibara, R Sakamoto, H Sasao, M Sasao, K Sato, S Satoh, T Satow, M Shoji, S Sudo, H Suzuki, M Takechi, N Tamura, S Tanahashi, K Tanaka, K Toi, T Tokuzawa, K Y Watanabe, T Watanabe, H Yamada, I Yamada, S Yamaguchi, S Yamamoto, K Yamazaki, M Yokoyama, Y Hamada, O Motojima, M Fujiwara
The Performance of ICRF Heated Plasmas in LHD Sep 2000
(IAEA-CN-77/EX8/4)

NIFS-661 K Yamazaki, K Y Watanabe, A Sagara, H Yamada, S Sakakibara, K Narihara, K Tanaka, M Osakabe, K Nishimura, O Motojima, M Fujiwara, the LHD Group,
Helical Reactor Design Studies Based on New Confinement Scalings Sep 2000
(IAEA-CN-77/ FTP 2/12)

NIFS-662 T Hayashi, N Mizuguchi, H Miura and T Sato,
Dynamics of Relaxation Phenomena in Spherical Tokamak Sep. 2000
(IAEA-CN-77THP2/13)

NIFS-663 H Nakamura and T Sato, H Kambe and K Sawada and T Saiki,
Design and Optimization of Tapered Structure of Near-field Fiber Probe Based on FDTD Simulation Oct 2000

NIFS-664 N Nakajima,
Three Dimensional Ideal MHD Stability Analysis in *L=2* Heliotron Systems Oct 2000

NIFS-665 S Fujiwara and T Sato,
Structure Formation of a Single Polymer Chain I Growth of trans Domains Nov 2000

NIFS-666 S Kida,
Vortical Structure of Turbulence· Nov 2000

NIFS-667 H Nakamura, S Fujiwara and T Sato,
Rigidity of Orientationally Ordered Domains of Short Chain Molecules Nov 2000

NIFS-668 T Mutoh, R Kumazawa, T Seki, K Saito, Y Torii, F Shimpo, G Nomura, T Watari, D A Hartmann, M Yokota, K Akaishi, N Ashikawa, P deVries, M. Emoto, H Funaba, M Goto, K. Ida, H. Idei, K. Ikeda, S. Inagaki, N Inoue, M. Isobe, O Kaneko, K Kawahata, A Komori, T Kobuchi, S Kubo, S Masuzaki, T Morisaki, S Morita, J Miyazawa, S Murakami, T Minami, S Muto, Y Nagayama, Y Nakamura, H Nakanishi, K Narihara, N Noda, K Nishimura, K Ohkubo, N Ohyabu, S Ohdachi, Y Oka, M. Osakabe, T Ozaki, B J Peterson, A Sagara, N Sato, S. Sakakibara, R Sakamoto, H Sasao, M Sasao, M Sato, T Shimozuma, M Shoji, S Sudo, H Suzuki, Y Takeiri, K Tanaka, K Toi, T Tokuzawa, K Tsumori, K Y Watanabe, I Watanabe, H Yamada, I Yamada, S Yamaguchi, K Yamazaki, M. Yokoyama, Y Yoshimura, Y. Hamada, O. Motojima, M Fujiwara.
Fast- and Slow-Wave Heating of Ion Cyclotron Range of Frequencies in the Large Helical Device Nov 2000

NIFS-669 K Mima, M S Jovanovic, Y Sentoku, Z-M Sheng, M M Skoric and T Sato,
Stimulated Photon Cascade and Condensate in Relativistic Laser-plasma Interaction Nov 2000

NIFS-670 L. Hadzievski, M M Skoric and T Sato,
On Origin and Dynamics of the Discrete NLS Equation Nov 2000

NIFS-671 K Ohkubo, S Kubo, H Idei, T Shimozuma, Y Yoshimura, F Leuterer, M Sato and Y Takita,
Analysis of Oversized Sliding Waveguide by Mode Matching and Multi-Mode Network Theory Dec 2000

NIFS-672 C Das, S. Kida and S. Goto,
Overall Self-Similar Decay of Two-Dimensional Tirbulence Dec 2000

NIFS-673 L A Bureyeva, T Kato, V S Lisitsa and C Namba,
Quasiclassical Representation of Autoionization Decay Rates in Parabolic Coordinates Dec 2000

NIFS-674 L.A Bureyeva V S Lisitsa and C. Namba,
Radiative Cascade Due to Dielectronic Recombination· Dec 2000

NIFS-675 M FHeyn, S V Kasilof, W Kernbichler, K Matsuoka, V V Nemov, S Okamura, O S Pavlichenko
Configurational Effects on Low Collision Plasma Confinement in CHS Heliotron/Torsatron, Jan 2001

NIFS-676 K. Itoh,
A Prospect at 11th International Toki Conference - Plasma physics, quo vadis? Jan 2001

NIFS-677 S Satake, H Sugama, M Okamoto and M Wakatani,
Classification of Particle Orbits near the Magnetic Axis in a Tokamak by Using Constants of Motion, Jan 2001

NIFS-678 M Tanaka and A Yu Grosberg,
Giant Charge Inversion of a Macroion Due to Multivalent Counterions and Monovalent Coions Molecular Dynamics Studyn, Jan 2001